Forward-angle elastic $\vec{p}p$ spin-depolarization and -rotation parameters at 0.8 GeV

M. L. Barlett, G. W. Hoffmann, J. A. McGill,* R. W. Fergerson, E. C. Milner, and J. A. Marshall
Department of Physics, The University of Texas at Austin, Austin, Texas 78712

J. F. Amann, B. E. Bonner, and J. B. McClelland
Los Alamos National Laboratory, Los Alamos, New Mexico 87545

(Received 6 February 1984)

800 MeV elastic $\vec{p}+p$ spin-depolarization and -rotation parameters D_{NN}, D_{SS}, D_{LL}, D_{SL}, and D_{LS} have been measured for the center-of-momentum angular range 4.8°—23.8° (0.26 $\text{fm}^{-1} \leq q \leq 1.28$ fm^{-1}). Statistical uncertainties are $\simeq \pm 0.01$—0.02 and total systematic uncertainty is $\leq \pm 0.035$. The data are in overall agreement with predictions from global phase shift analysis.

I. INTRODUCTION

In recent years a considerable effort has been made to provide data which allow a complete determination of the pp elastic phase shifts and amplitudes at energies near 800 MeV. The interest in such work stems from the energy-dependent structure seen in certain nucleon-nucleon observables[1–3] and from the need for precisely determined amplitudes required by microscopic models for nuclear physics applications.[4–9]

An examination of the pp data base[10–20] reveals, however, that no spin-depolarization and -rotation parameters have been measured for momentum transfer $q \leq 1$ fm^{-1} at energies near 800 MeV, although precise differential cross section and analyzing power data do exist. It is important to have such data in order to check, and possibly improve, the accuracy of phase shift solutions at small momentum transfer.

Here we report results of precise measurements (statistical errors $\simeq \pm 0.01$—0.02; total systematic error $\leq \pm 0.035$) of the spin-depolarization and -rotation parameters D_{ij} (D_{NN}, D_{SS}, D_{LL}, D_{SL}, and D_{LS}) for 800 MeV $\vec{p}+p$ elastic scattering over the momentum transfer region 0.26 $\text{fm}^{-1} \leq q \leq 1.28$ fm^{-1} ($4.8° \leq \theta_{\text{c.m.}} \leq 23.8°$). The D_{NN}, D_{SS}, and D_{LS} data at 23.8° are consistent with data measured by McNaughton *et al.*[10] near this angle. The data are in basic agreement with predictions from global phase shift analysis.

II. EXPERIMENTAL

The data were obtained at the Los Alamos Clinton P. Anderson Meson Physics Facility (LAMPF) using the high resolution spectrometer (HRS) and the HRS focal plane polarimeter (FPP). During three serial running periods, beams of 800±2 MeV polarized protons ($\hat{n}$, $\hat{s}$, and $\hat{l}$ type; see Fig. 1 for coordinate system definitions) bombarded a liquid hydrogen (LH_2) target located at the center of the 1 m radius scattering chamber. The target flask was a 3.8 cm diameter vertical Mylar cylinder of 0.08 mm wall thickness. Two ion chambers located inside the scattering chamber 0.75 m downstream of the target monitored integrated beam current.

A beam line polarimeter located 10 m upstream of the HRS scattering chamber determined beam polarization for the $\hat{n}$ and $\hat{s}$ type beams and served as a monitor of the polarization orientation (i.e., null $\hat{n}$ and $\hat{s}$ components) for the $\hat{l}$ type beam. Quench ratio[13] measurements of the beam polarization magnitude also were made continuously during the course of the experiment. Beam polarization was typically 75%. For each type of beam, normal (N) and reverse (R) directions [$\hat{n}$: up (N), down (R); $\hat{s}$: left (N), right (R); $\hat{l}$: parallel (N), antiparallel (R) to incident momentum; see Fig. 1] were changed at the ion source every minute; logic levels from the source were read by the HRS on-line data acquisition system and used to tag each recorded event according to beam spin orientation.

Target-scattered protons were momentum analyzed by the HRS, a missing-mass spectrometer described elsewhere,[21] and rescattered by the FPP carbon analyzer target to determine polarization components at the focal plane. An extra scintillator (SX) was used with the stan-

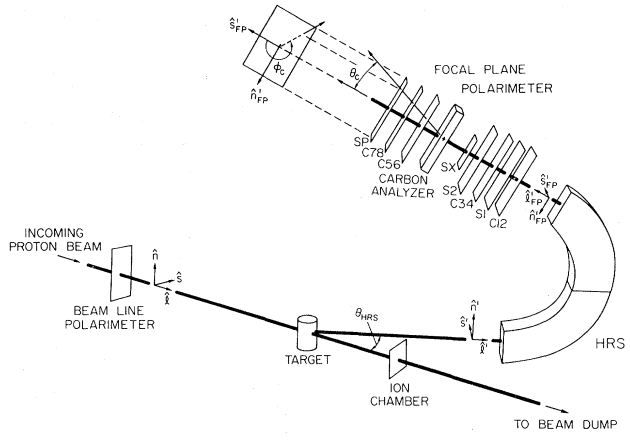

FIG. 1. A schematic drawing of the experimental setup showing the major components of the HRS FPP system. The various coordinate systems are consistent with the equations in the text. Note that the portion of the figure defining ϕ_c is a view of scintillator SP looking along the optic axis towards the HRS.

dard HRS focal plane scintillator system to restrict the focal plane momentum acceptance to $\Delta p/p \simeq \pm 0.6\%$. The basic HRS FPP detector arrangement is shown schematically in Fig. 1. For on-line data acquisition, an event was defined as a fourfold coincidence among scintillators *S*1, *S*2, *SX*, and *SP*. For each event the two-dimensional multiwire drift chambers *C*12 and *C*34 provided trajectory position and angle information at the HRS focal plane, while the two-dimensional multiwire drift chambers *C*56 and *C*78 provided position and angle information for trajectories of protons scattered by the FPP carbon analyzer. The carbon analyzer thickness was chosen to optimize the FPP performance (multiple Coulomb scattering and the cross-section—analyzing-power product must be considered); this thickness varied between 24—27 cm depending upon the HRS scattering angle.

The data acquisition system consisted of a buffered CAMAC system of time-to-digital converters (TDC's) and analog-to-digital converters (ADC's) interfaced through a microprogrammable branch driver (MBD) to a PDP 11/45 computer. For each event, wire chamber timing information and scintillator time and pulse height information were written on magnetic tape for off-line analysis. Fast tests on the FPP raw data (drift chamber timing information) were made in the MBD to select for taping only those events which scattered more than $\simeq 3°$ in the FPP carbon analyzer. Typically 50% of the events were rejected in the MBD. The FPP and associated hardware are discussed at length elsewhere.[22]

The FPP determines polarization components $P_{n',\mathrm{FP}}$ and $P_{s',\mathrm{FP}}$ (see Fig. 1), which are orthogonal to the optic axis of the spectrometer at the focal plane. Since the FPP is located downstream of the HRS dipoles, spin components at the target which are not parallel to the HRS fields, precess while traversing the spectrometer. This feature enables measurement of polarization components which are longitudinal (parallel or antiparallel to the particles's momenta) at the target.

Using the setup described above, data were obtained at HRS laboratory scattering angles 2°, 3°, 6°, and 10° for $\hat{n}$ and $\hat{s}$ type beams and at 3°, 6°, and 10° for the $\hat{l}$ type beam. Empty flask runs were made at 2° and 3° to aid in a better determination of flask generated backgrounds.

III. DATA ANALYSIS

A. General

Using the method of Besset *et al.*,[23] the laboratory angular distribution $I(\theta_c,\phi_c)$ of protons after scattering in the FPP carbon analyzer is given by

$$I(\theta_c,\phi_c)=k\left[\frac{d\sigma}{d\Omega}\right]_c [1+P_{n',\mathrm{FP}}A_c(\theta_c)\cos\phi_c - P_{s',\mathrm{FP}}A_c(\theta_c)\sin\phi_c]A(\theta_c,\phi_c)\,. \quad (1)$$

Here, θ_c and ϕ_c are the polar and azimuthal scattering angles in the carbon analyzer, respectively (see Fig. 1); k is a normalization factor, while $(d\sigma/d\Omega)_c$ and $A_c(\theta_c)$ are the p-^{12}C unpolarized inclusive differential cross section and $\vec{p}$-^{12}C inclusive analyzing power, respectively; $P_{n',\mathrm{FP}}$ and $P_{s',\mathrm{FP}}$ are the $\hat{n}'_{\mathrm{FP}}$ and $\hat{s}'_{\mathrm{FP}}$ polarization components at the carbon analyzer, respectively; and $A(\theta_c,\phi_c)$ is the instrumental acceptance. If $A_c(\theta_c)$ is known and $I(\theta_c,\phi_c)$ is measured, then Fourier analysis or weighted sums techniques[23] allow determination of $P_{n',\mathrm{FP}}$ and $P_{s',\mathrm{FP}}$.

$A_c(\theta_c)$ is a function of the proton energy (766—798 MeV for this experiment) and was calculated from an empirical energy-dependent parametrization[24] of a global data base from Tri-University Meson Facility (TRIUMF), Schweizerisches Institute Für Nuklearforschung (SIN), and LAMPF. During the course of the experiment, $A_c(\theta_c)$ data were obtained at 733 and 800 MeV and used to check the accuracy of this parametrization; these data were obtained by running an $\hat{s}$ type polarized beam through the HRS FPP system at 0° HRS laboratory angle. Figure 2 shows the experimental results obtained using the HRS-FPP; the predicted carbon analyzing powers from Ref. 24 are also shown (solid curves).

The 800 MeV HRS $A_c(\theta_c)$ data, using *analyzing powers* from the energy-dependent parametrization, yielded an *average* carbon analyzing power (averaged over a polar angular range of 4.5°—20°) which was 3.8% lower than the *average* analyzing power obtained from the HRS data (averaged in the same manner). This difference in average analyzing power is somewhat greater than the systematic uncertainty (2—3%) quoted for the energy-dependent

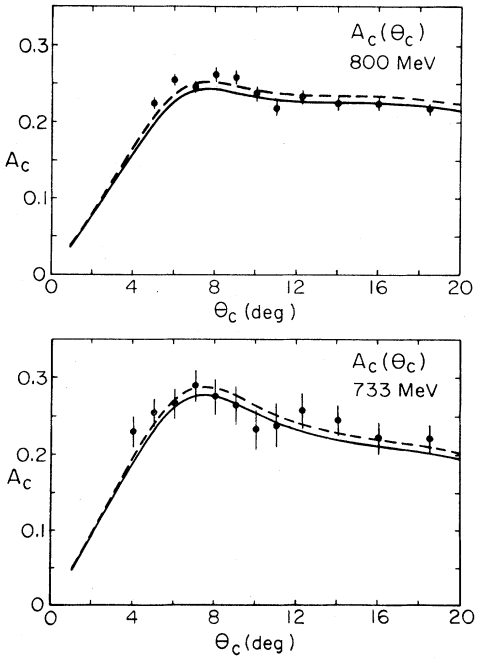

FIG. 2. The $\vec{p}$-^{12}C inclusive analyzing power data at $E_p=733$ and 800 MeV obtained using the HRS FPP are compared to the energy dependent parametrization (solid curves) of Ref. 24. The dashed curves are the corrected (3.8% correction) analyzing powers used in the analysis (see the text). The angle θ_c is measured in the laboratory as shown in Fig. 1.

parametrization.[24] However, a more recent[25] unpublished energy-dependent empirical fit to an expanded $A_c(\theta_c)$ data base is consistent with the 3.8% difference observed here. The dashed curves in Fig. 2 show the correction (3.8%) to the parametrization of Ref. 24 that was used in the off-line analysis of the data.

The $\hat{n}'$ and $\hat{l}'$ components of the target-scattered proton's spin precess when passing through the HRS dipoles, while the $\hat{s}'$ component does not (to first order). Thus, in general, the measured polarization component at the focal plane $P_{n',\mathrm{FP}}$ is related to both the $\hat{n}'$ and $\hat{l}'$ polarizations at the target. The precession angle χ is given by

$$\chi=\gamma\left[\frac{g}{2}-1\right]\alpha\simeq 269\gamma\ , \tag{2}$$

where γ is the Lorentz factor, $g/2$ is the proton magnetic moment, and α is the bend angle (about 150° for the HRS). To first order the $\hat{n}'$ and $\hat{l}'$ polarization components at the target are given by $P_{n'}=P_{n',\mathrm{FP}}/\cos(\chi)$ and $P_{l'}=P_{n',\mathrm{FP}}/\sin(\chi)$.

Using the above information and correcting for out of plane scattering, to first order the spin-depolarization parameter (Wolfenstein triple scattering parameter D) is given by

$$D=D_{nn'}=D_{NN}=\frac{(P^{+}_{n',\mathrm{FP}}-P^{-}_{n',\mathrm{FP}})+P_B(\hat{n})A_y\cos(\xi)(P^{+}_{n',\mathrm{FP}}+P^{-}_{n',\mathrm{FP}})}{2\cos(\chi)\cos^2(\xi)P_B(\hat{n})}\ , \tag{3a}$$

or alternately,

$$D=D_{nn'}=D_{NN}=\frac{P^{+}_{n',\mathrm{FP}}-P^{-}_{n',\mathrm{FP}}}{2\cos^2(\xi)\cos(\chi)P_B(\hat{n})}[1-P_B^2(\hat{n})A_y^2\cos^2(\xi)]+A_y^2\ , \tag{3b}$$

and the spin-rotation parameters (Wolfenstein triple scattering parameters R, R', A, and A') are given by

$$R=D_{ss'}=D_{SS}=\frac{P^{+}_{s',\mathrm{FP}}-P^{-}_{s',\mathrm{FP}}}{2P_B(\hat{s})\cos^2(\xi)}[1-P_B(\hat{s})A_y\sin(\xi)]\ , \tag{4}$$

$$R'=D_{sl'}=D_{SL}=\frac{P^{+}_{n',\mathrm{FP}}-P^{-}_{n',\mathrm{FP}}}{2P_B(\hat{s})\cos(\xi)\sin\chi}[1-P_B(\hat{s})A_y\sin(\xi)]\ , \tag{5}$$

$$A=D_{ls'}=D_{LS}=\frac{P^{+}_{s',\mathrm{FP}}-P^{-}_{s',\mathrm{FP}}}{2P_B(\hat{l})\cos(\xi)}\ , \tag{6}$$

and

$$A'=D_{ll'}=D_{LL}=\frac{P^{+}_{n',\mathrm{FP}}-P^{-}_{n',\mathrm{FP}}}{2P_B(\hat{l})\sin(\chi)}\ . \tag{7}$$

Here, $P^{\pm}_{n',\mathrm{FP}}$ and $P^{\pm}_{s',\mathrm{FP}}$ are the measured polarizations in the $\hat{n}_{\mathrm{FP}}$ and $\hat{s}_{\mathrm{FP}}$ directions [the + (−) indicates normal (reverse) beam polarization], $P_B(\hat{n}$, $\hat{s}$, or $\hat{l})$ is the incident beam polarization in the $\hat{n}$, $\hat{s}$, or $\hat{l}$ direction, A_y is the analyzing power, ξ is the average out-of-plane scattering angle at the target (horizontal scattering plane; see Fig. 1), and χ is the average precession angle. It is assumed that P_B^{+} (normal) $=-P_B^{-}$ (reverse) $=P_B$ and that the sines and cosines of ξ and χ are averaged over the events. Equations (4)—(7) show that FPP instrumental asymmetries cancel to first order when D_{SS}, D_{SL}, D_{LL}, and D_{LS} are calculated. Equation (3b) shows that a knowledge of the $\vec{p}+p$ analyzing power, A_y, allows a determination of D_{NN} that is independent of FPP instrumental asymmetries.

B. Off-line data reduction and results

A pulse height (from scintillator $S2$ in Fig. 1) versus time-of-flight (between $S2$ and SP in Fig. 1) particle identification (PID) scheme identified protons scattered at the target, and a gate on the missing-mass spectrum (see Fig. 3) selected elastically scattered protons for p + p. Events were rejected unless the scattering in the FPP was for a polar angle θ_c such that $4.5°\leq\theta_c\leq 20°$. The upper limit is a physical constraint of the FPP while the lower limit eliminated events which fell within the multiple Coulomb scattering region or which did not scatter in the carbon analyzer. An additional test on the particle's trajectory ensured that the scattering took place in the FPP carbon analyzer and that the distance of closest approach between the trajectory before and after the carbon scatterer was reasonable. Typically, 25—35% of the taped events passed the various FPP tests; these *good FPP events* were then subjected to two FPP acceptance tests in order to minimize instrumental (false) asymmetries. These tests, known as the "$\phi+\pi$" test, and the "cone" test, are dis-

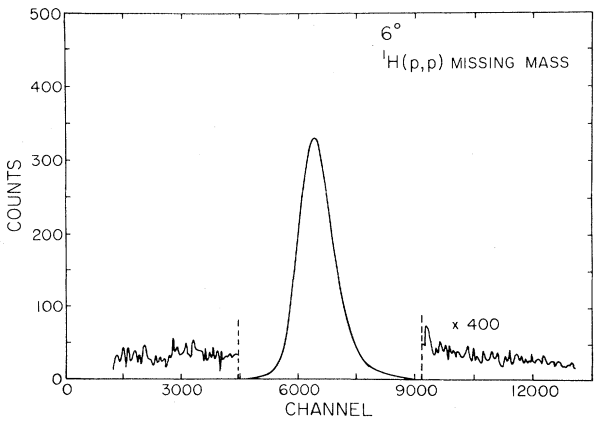

FIG. 3. The ^{1}H(p,p) missing mass spectrum obtained at 6°. The vertical scale is arbitrary while the horizontal scale is such that the peak is about 1 MeV wide (FWHM).

cussed in detail elsewhere.[22,23] The $\phi+\pi$ test requires that, given the polar and azimuthal scattering angles (θ_c,ϕ_c) in the carbon analyzer, scattering angles $(\theta_c,\phi_c+\pi)$ must fall within the instrumental acceptance or the event is rejected. The more restrictive cone test requires that given a polar scattering angle, θ_c, for the event to be valid, all azimuthal scattering angles $(0\leq\phi_c\leq 2\pi)$ must lie within the acceptance. These tests were applied to the data in parallel (i.e., polarizations were computed for events which passed either test). Typically, 97% (93%) of the good FPP events passed the $\phi+\pi$ (cone) test.

Corrections were made to the measured polarizations due to background under the hydrogen elastic peak in the missing mass spectrum [primarily the straggling tail from $\vec{p}+{}^{12}C$ elastic scattering (2° and 3° runs) and $\vec{p}+{}^{12}C$ quasielastic scattering due to ^{12}C in the Mylar flask]. The background-corrected polarizations were obtained from

$$P^{\pm}_{n',\mathrm{FP}}=\frac{(1+r^{\pm})P^{(\pm)t}_{n',\mathrm{FP}}-P^{(\pm)b}_{n',\mathrm{FP}}}{r^{\pm}} \tag{8}$$

and

$$P^{\pm}_{s',\mathrm{FP}}=\frac{(1+r^{\pm})P^{(\pm)t}_{s',\mathrm{FP}}-P^{(\pm)b}_{s',\mathrm{FP}}}{r^{\pm}}\ , \tag{9}$$

where $P^{(\pm)t}_{n',\mathrm{FP}}$ and $P^{(\pm)t}_{s',\mathrm{FP}}$ are the peak plus background polarizations, $P^{(\pm)b}_{n',\mathrm{FP}}$ and $P^{(\pm)b}_{s',\mathrm{FP}}$ are background polarizations, and $r^{\pm}$ are the peak to background ratios for the region of the missing mass spectrum used to determine $P^{(\pm)t}_{n',\mathrm{FP}}$ and $P^{(\pm)t}_{s',\mathrm{FP}}$ for normal $(+)$ and reverse $(-)$ beam spin directions, respectively. This technique is dicussed in Refs. 22 and 23.

The background under the ^{1}H(p,p) elastic peak in the missing mass spectrum varied between 0.5—5.0% for all data (except for the $\hat{s}$ type run at 2.0° lab where the background was 11.8%). A typical missing mass spectrum, showing the hydrogen elastic peak and the background, is shown in Fig. 3. Since background polarizations tended to be very similar to the peak plus background polarizations, the difference between each D_{ij} obtained with and without background correction was small (typically between 0—0.02).

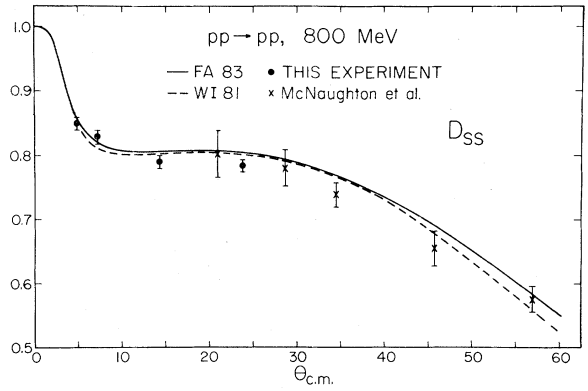

FIG. 5. The spin-rotation parameter D_{SS} for $\vec{p}$p at 800 MeV. Also shown are data from Ref. 10 and phase shift solutions from Ref. 26 (see the text).

For the $\hat{n}$-type runs, the beam polarization was determined from the normal-reverse asymmetries measured by the HRS (2°, 3°, 6°, and 10°), and the known $\vec{p}$ + p analyzing powers [pp phase shift solution *SM*82 (Ref. 26)]. The beam polarizations obtained in this way allowed an accurate determination of the analyzing power of the beam line polarimeter. The polarimeter monitored the up-down and left-right asymmetries for $\vec{p}+C_{10}H_{11}\rightarrow p+p+X$ by detecting the two protons at conjugate angles corresponding to p + p→p + p elastic kinematics at $\theta_{c.m.}\simeq 45°$. The polarimeter analyzing power was determined to be $0.449\pm 1\%$. For the $\hat{n}$ and $\hat{s}$ beams, polarizations determined by the beam line polarimeter agreed with those determined from the quench ratio measurements at the level of $\simeq\pm 1\%$. In the final analysis, beam polarizations given by the beam line polarimeter were used for $\hat{n}$ and $\hat{s}$ type beams while the quench ratio polarizations were used for the $\hat{l}$ type beam.

The resulting spin-depolarization and -rotation parameters, obtained using cone test polarizations and Eqs. (3b)—(7), are shown in Figs. 4—8 and listed in Table I; differences between these values and those computed us-

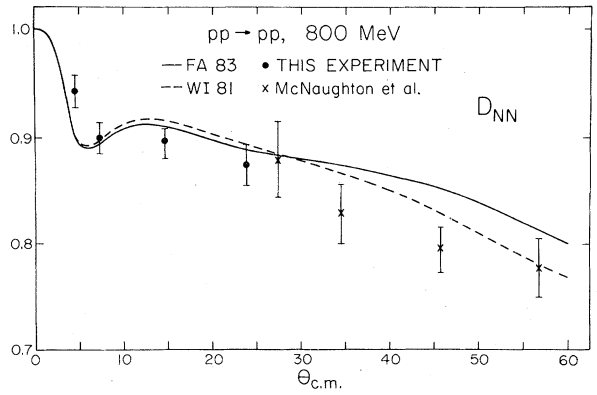

FIG. 4. The spin-depolarization parameter D_{NN} for $\vec{p}$p at 800 MeV. Also shown are data from Ref. 10 and phase shift solutions from Ref. 26 (see the text).

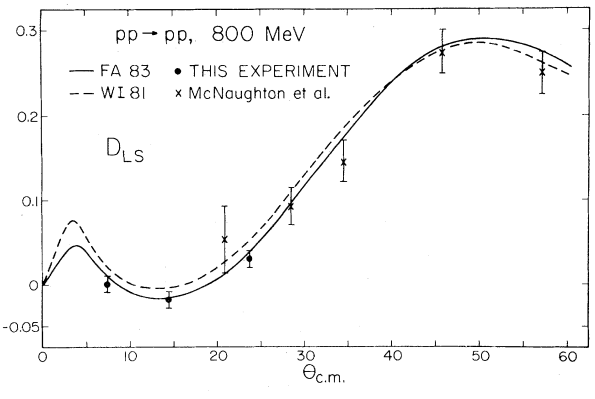

FIG. 6. The spin-rotation parameter D_{LS} for $\vec{p}$p at 800 MeV. Also shown are data from Ref. 10 and phase shift solutions from Ref. 26 (see the text).

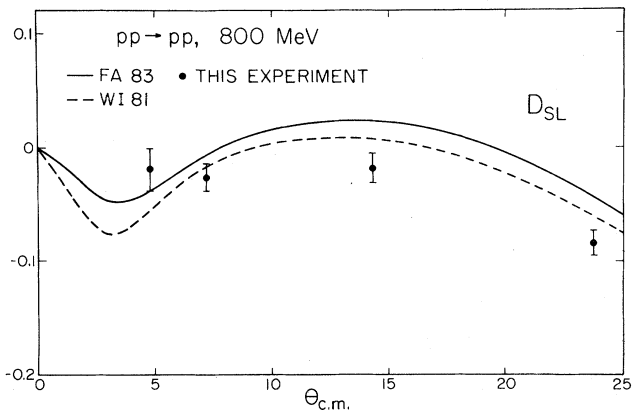

FIG. 7. The spin-rotation parameter D_{SL} for $\vec{p}p$ at 800 MeV. Also shown are phase shift solutions from Ref. 26 (see the text).

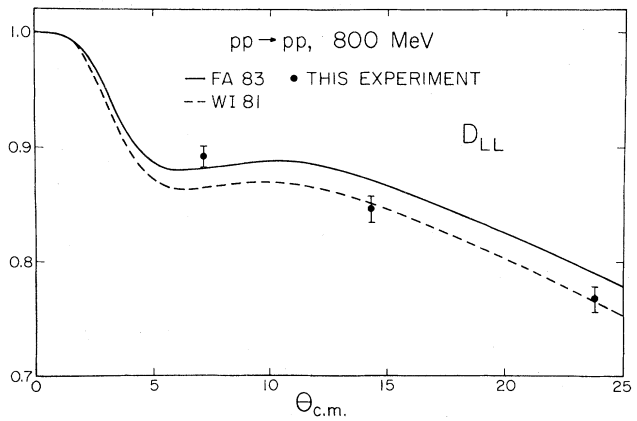

FIG. 8. The spin-rotation parameter D_{LL} for $\vec{p}p$ at 800 MeV. Also shown are phase shift solutions from Ref. 26 (see the text).

ing $\phi+\pi$ test polarizations are quite small ($\lesssim 1\%$), in general. The analyzing powers used in Eqs. (3b), (4), and (5) were taken from the phase shift solution *SM*82 (Ref. 26) which accurately reproduces a vast amount of $\sim$800 MeV analyzing power data. The numerical values are the results of averaging over the full angular acceptance of the HRS and are plotted and tabulated at the central angle of the spectrometer (HRS acceptance $\simeq\pm 1°$, plane of scattering; $\simeq\pm 2°$, out of plane). Also shown in Figs. 4–8 are some of the data of McNaughton *et al.*[10] and results from phase shift analysis[26] to be discussed in Sec. IV.

TABLE I. Elastic spin-depolarization and -rotation parameters for $\vec{p}p$ at 800 MeV.

θ_{lab} (deg)	$\theta_{c.m.}$ (deg)	D_{NN}	ΔD_{NN}
2.0	4.8	0.943	0.016
3.0	7.2	0.902	0.015
6.0	14.3	0.888	0.016
10.0	23.8	0.875	0.020
θ_{lab} (deg)	$\theta_{c.m.}$ (deg)	D_{SS}	ΔD_{SS}
2.0	4.8	0.848	0.012
3.0	7.2	0.828	0.010
6.0	14.3	0.792	0.010
10.0	23.8	0.785	0.010
θ_{lab} (deg)	$\theta_{c.m.}$ (deg)	D_{SL}	ΔD_{SL}
2.0	4.8	−0.018	0.018
3.0	7.2	−0.026	0.014
6.0	14.3	−0.019	0.014
10.0	23.8	−0.084	0.012
θ_{lab} (deg)	$\theta_{c.m.}$ (deg)	D_{LS}	ΔD_{LS}
3.0	7.2	0.000	0.009
6.0	14.3	−0.019	0.008
10.0	23.8	0.031	0.011
θ_{lab} (deg)	$\theta_{c.m.}$ (deg)	D_{LL}	ΔD_{LL}
3.0	7.2	0.893	0.014
6.0	14.3	0.847	0.012
10.0	23.8	0.768	0.014

C. Systematic uncertainties

The assigned errors reflect statistical uncertainties, uncertainties in the background determination and subtraction, the statistical determination of the incident beam polarization, and for D_{NN}, D_{SS}, and D_{SL}, an uncertainty[26] in the analyzing power A_y of ± 0.01 [see Eqs. (3b), (4), and (5)]. Systematic uncertainties not reflected in these errors are discussed below.

The largest systematic uncertainty relates to the energy-dependent analyzing powers $[A_c(\theta_c)]$ used for the FPP carbon analyzer. As discussed in Sec. III A, comparison of the event-averaged analyzing power for the 800 MeV $\vec{p}$-^{12}C inclusive data obtained with the HRS FPP with the same quantity using analyzing powers from the energy-dependent fit to the global data base led to a 3.8% correction to the focal plane polarizations. Although it was only possible to perform this check at one energy due to the lack of accurate data at other energies spanned by the experiment, $\vec{p}$-^{12}C inclusive data obtained using the HRS FPP at lower energies (300–500 MeV) show that the energy dependence of the fit is essentially correct. We believe that the systematic uncertainty of the inclusive carbon analyzing power is small ($\lesssim \pm 2.0\%$) and introduces uncertainty into the D_{ij} results of $\lesssim \pm 0.02$.

Uncertainty in the absolute beam polarization is another source of systematic error not included. This uncertainty is estimated to be $\pm 1\%$ based on previous studies of the quench ratio technique[19,27] and beam line polarimeter-quench monitor consistency. Therefore the effect on each D_{ij} is $\lesssim \pm 0.01$.

Instrumental asymmetries inherent in the FPP can also lead to false asymmetries. However, measurement of the polarizations with normal *and* reverse incident beam spins

facilitates computation [Eqs. (3b)—(7)] of the spin-depolarization and -rotation parameters such that false asymmetries cancel to first order. However, instrumental asymmetries do not cancel in the first order expressions[22] for the *induced polarization P*. Comparison of the calculated P with the known[26] P at each angle indicated that instrumental asymmetries from run to run were typically $\leq \pm 0.01$. A careful examination of the FPP calibration data obtained at 0° also led to false asymmetries consistent with zero within statistical determination ($\leq \pm 0.01$).

Systematic effects due to out-of-plane scattering and misalignment of the incident beam spin orientation have been investigated in detail in Ref. 22; they are negligible in this experiment (typically the average out of plane scattering angle ξ was $0 \pm 0.1°$, and incident beam spin orientations were aligned to $\pm 2°$—$3°$). Omission of higher order terms in the expressions for the triple scattering parameters also has an insignificant effect. We believe that the major systematic effects have been considered and that total systematic uncertainty is about ± 0.035 or less.

Since only three of the four parameters obtained with $\hat{s}$ and $\hat{l}$ type beams are independent, an angle-to-angle consistency test was made as an additional check of the data. This was done using the expression[28]

$$\tan(\theta_{\text{lab}}) = \frac{D_{SL} + D_{LS}}{D_{LL} - D_{SS}} , \tag{10}$$

where θ_{lab} is the laboratory scattering angle. D_{NN} is independent of the other parameters and is unconstrained by any expression of the above type. Using the values of D_{LL}, D_{SS}, and D_{LS} obtained from the experiment, D_{SL} was calculated at 3°, 6°, and 10° using Eq. (10). Statistical errors and an overall systematic error of ± 0.035 were included, and the calculated values of D_{SL} were compared to the experimental values. The data and calculated values were found to agree within errors at all angles.

IV. SUMMARY AND CONCLUSIONS

The experiment provided precise 800 MeV elastic $\vec{p} + p$ spin-depolarization and -rotation data (D_{NN}, D_{SS}, D_{LL}, D_{SL}, and D_{LS}) for momentum transfers $0.26\ \text{fm}^{-1} \leq q \leq 1.28\ \text{fm}^{-1}$ ($4.8° \leq \theta_{\text{c.m.}} \leq 23.8°$) for comparison with results from global phase shift analysis. The statistical uncertainties in the D_{ij} are $\simeq \pm 0.01$—0.02, while the total systematic uncertainty is believed to be $\leq \pm 0.035$. The data are presented in Figs. 4—8 and Table I. The D_{NN}, D_{SS}, and D_{LS} data at 23.8° are consistent with the data of McNaughton *et al.*[10] near this angle; this consistency is another indication that the overall systematic error is small. The solid curves of Figs. 4—8 are from a recent phase shift solution generated by Arndt *et al.*;[26] the data reported here *are included* in the fit. Also shown (dashed curves) are results[26] from a preexisting solution (*WI*81). As seen in the figures, overall agreement between both phase shift solutions and the new data is good, although additional data may be required to improve the accuracy of the phase shift analysis.

This work was supported in part by the U.S. Department of Energy and The Robert A. Welch Foundation.

*Present address: Los Alamos National Laboratory, Los Alamos, NM 87545.

[1]I. P. Auer *et al.*, Phys. Lett. **70B**, 475 (1977).
[2]K. Hidaka *et al.*, Phys. Lett. **70B** 479 (1977).
[3]N. Hoshizaki, Prog. Theor. Phys. **60**, 1796 (1978); **61**, 129 (1979).
[4]L. Ray *et al.*, Phys. Rev. C **23**, 828 (1981).
[5]L. Ray, W. R. Coker, and G. W. Hoffmann, Phys. Rev. C **18**, 2641 (1978).
[6]G. W. Hoffmann *et al.*, Phys. Rev. Lett. **47**, 1436 (1981).
[7]A. K. Kerman, H. McManus, and R. M. Thaler, Ann. Phys. (N.Y.) **8**, 551 (1959).
[8]L. Ray, in *The Interaction Between Medium Energy Nucleons in Nuclei (Indiana University, 1982),* Proceedings of the Workshop on the Interaction Between Medium Energy Nucleons in Nuclei, AIP Conf. Proc. No. 97, edited by H. O. Meyer (AIP, New York, 1983), p. 121.
[9]B. C. Clark, S. Hama, R. L. Mercer, L. Ray, and B. D. Serot, Phys. Rev. Lett. **50**, 1644 (1983).
[10]M. W. McNaughton *et al.*, Phys. Rev. C **25**, 1967 (1982).
[11]H. B. Willard *et al.*, Phys. Rev. C **14**, 1545 (1976).
[12]P. R. Bevington *et al.*, Phys. Rev. Lett. **41**, 384 (1978).
[13]M. W. McNaughton *et al.*, Phys. Rev. C **23**, 1128 (1981).
[14]F. Irom, G. J. Igo, J. B. McClelland, and C. A. Whitten, Jr., Phys. Rev. C **25**, 373 (1982).
[15]A. Wriekat *et al.*, Phys. Lett. **97B**, 33 (1980); G. Pauletta *et al.*, Phys. Rev. C **27**, 282 (1983).
[16]M. W. McNaughton *et al.*, Phys. Rev. C **23**, 838 (1981).
[17]D. A. Bell *et al.*, Phys. Lett. **94B**, 310 (1980).
[18]I. P. Auer *et al.*, Phys. Rev. Lett. **41**, 1436 (1978).
[19]M. L. Barlett *et al.*, Phys. Rev. C **27**, 682 (1983).
[20]V. A. Andreev *et al.*, Gatchina Laboratory Report No. 656, 1981 (unpublished).
[21]B. Zeidman, Los Alamos National Laboratory Report LA-4773-MS, 1971 (Part I unpublished).
[22]J. B. McClelland, J. F. Amann, W. D. Cornelius, H. A. Thiessen, and B. Aas, Nucl. Instrum. Methods (to be published).
[23]D. Besset *et al.*, Nucl. Instrum. Methods **166**, 515 (1979).
[24]R. D. Ransome *et al.*, Nucl. Instrum. Methods **201**, 315 (1982).
[25]D. J. Cremans, Masters thesis, University of Texas at Austin, 1983 (unpublished).
[26]R. A. Arndt *et al.*, Phys. Rev. D **28**, 97 (1983); (private communication).
[27]M. W. McNaughton and E. P. Chamberlin, Phys. Rev. C **24**, 1778 (1981).
[28]J. Bystricky, F. Lehar, and P. Winternitz, J. Phys. (Paris) **39**, 1 (1978).